Supporting Information

A Class of Catalysts of BiOX (X=Cl, Br, I) for Anchoring Polysulfides and Accelerating Redox Reaction in Lithium Sulfur Batteries

Xian Wu,[†] Nannan Liu,[†] Maoxu Wang,[†] Yue Qiu[†] Bin Guan,[†] Da Tian,[†] Zhikun Guo,[†] Lishuang Fan,[‡] Naiqing Zhang,[†,‡*]*

[†] School of Chemistry and Chemical Engineering; State Key Laboratory of Urban Water Resource and Environment, Harbin Institute of Technology, Harbin 150001 (China)

[‡]Academy of Fundamental and Interdisciplinary Sciences, Harbin Institute of Technology Harbin, 150001 (China)

Supplementary Figures and Tables

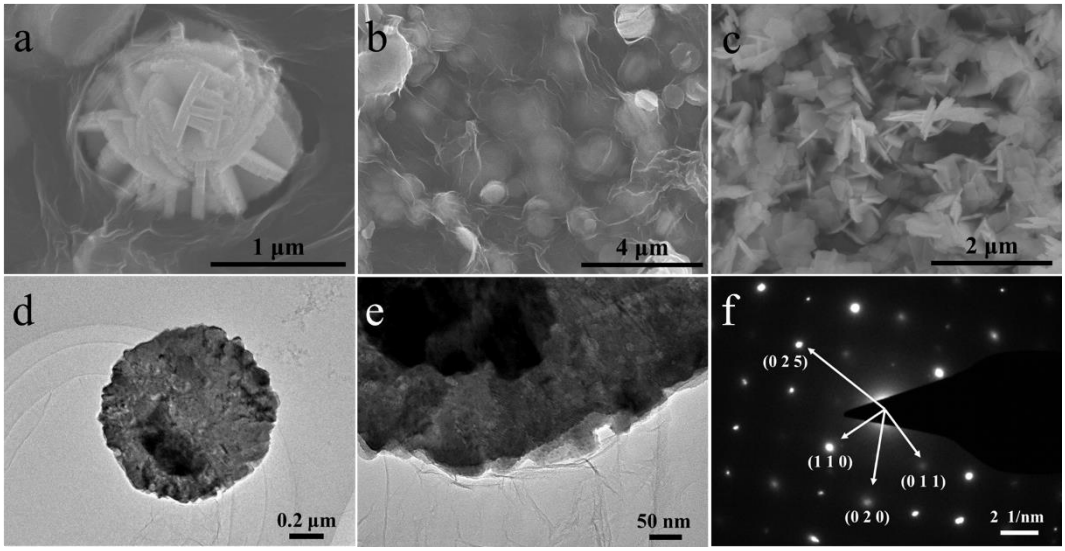

Figure S1. SEM images of (a, b) BiOCl/G with different magnifying scale, and bare BiOCl without rGO. (d, e) TEM images of BiOCl/G with different magnifying scale. (f) SAED pattern of BiOCl/G.

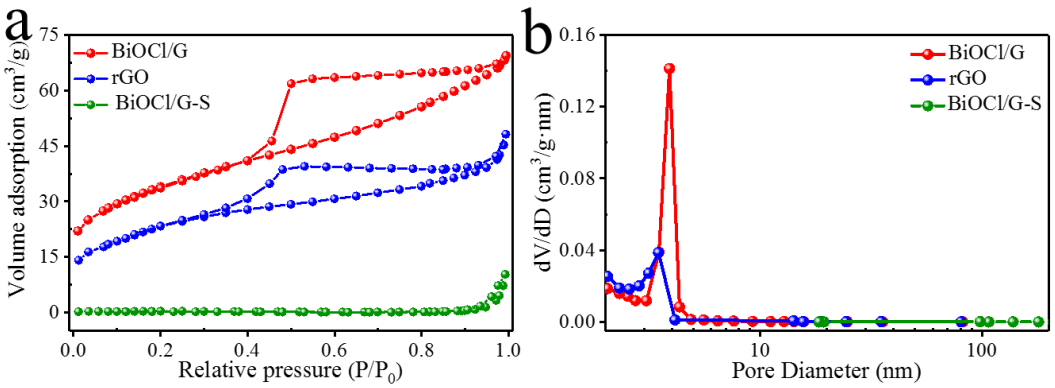

Figure S2. (a) N_2 adsorption/desorption isotherms, and (d) pore size distribution curves of BiOCl/G, rGO and BiOCl/G-S.

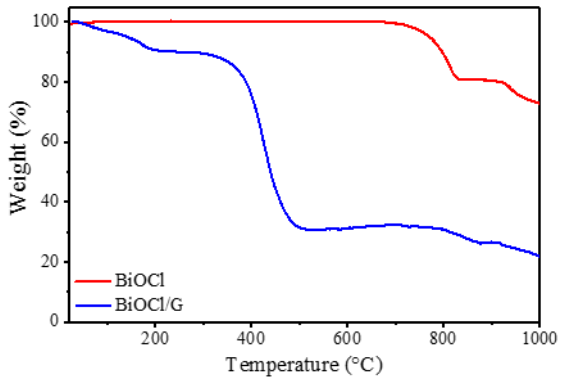

Figure S3. TGA curves of BiOCl and BiOCl/G

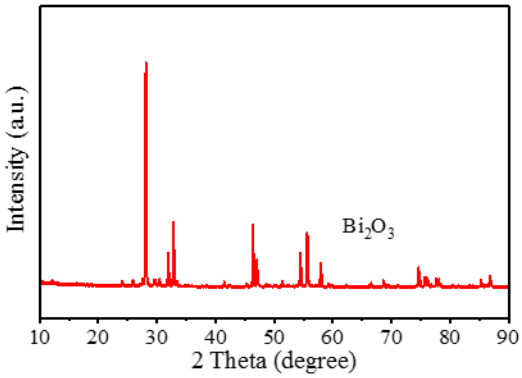

Figure S4. XRD pattern of residue after TGA test.

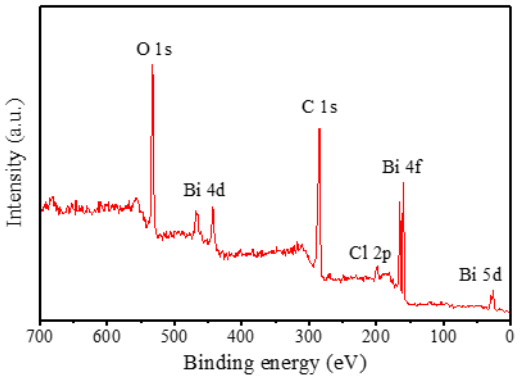

Figure S5. Survey XPS spectra of BiOCl/G.

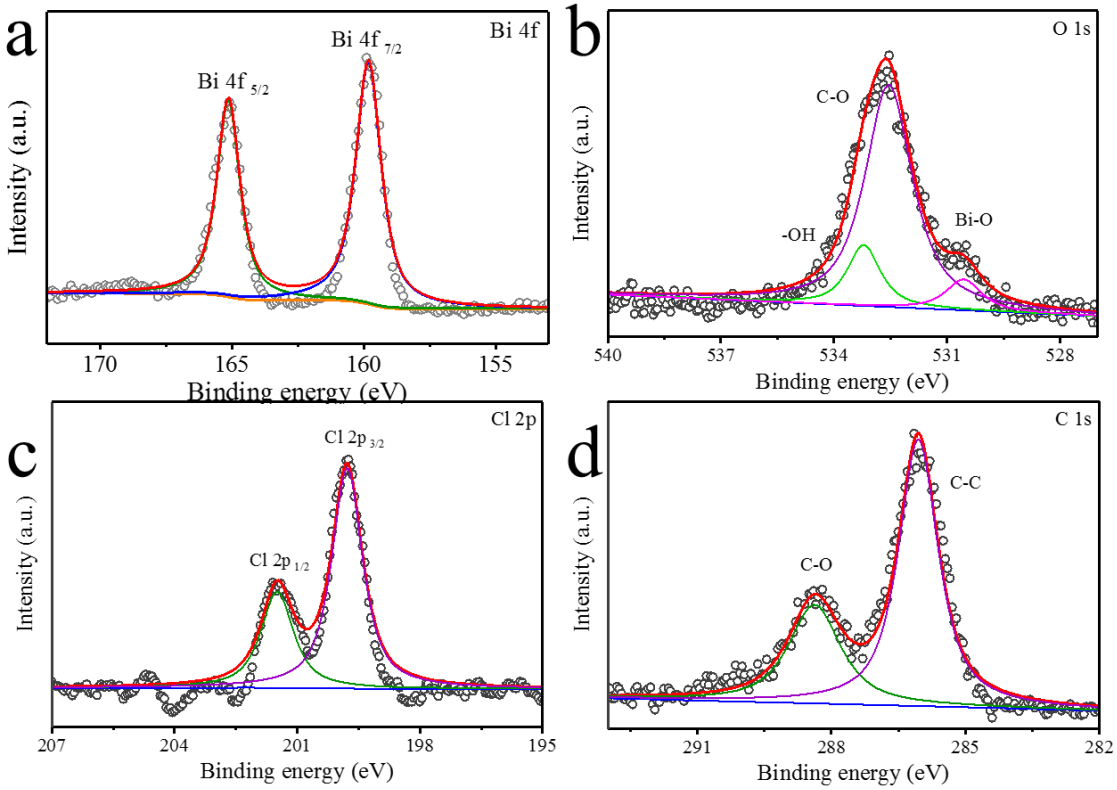

Figure S6. XPS spectra of (a) Bi 4d, (b) O 1s, (c) Cl 2p, and (d) C 1s.

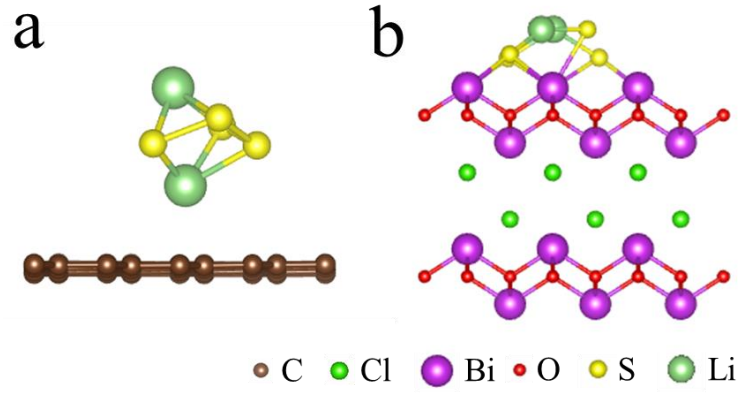

Figure S7. Side sectional view of optimized structures for Li_2S_4 adsorbed on (a) graphene and (b) BiOCl.

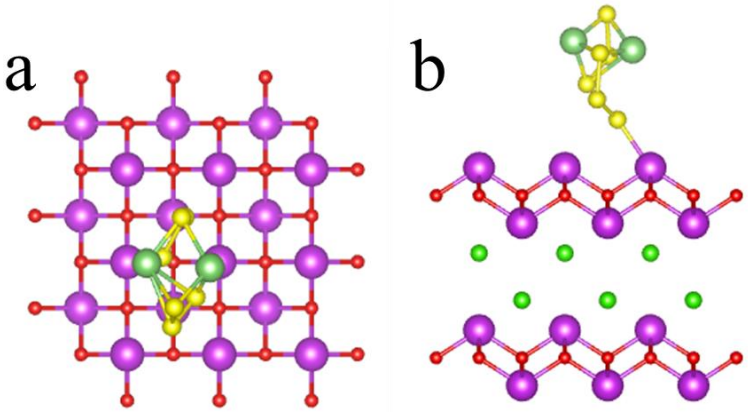

Figure S8. (a) Top and (b) side sectional views of optimized structures for Li_2S_6 adsorbed on BiOCl.

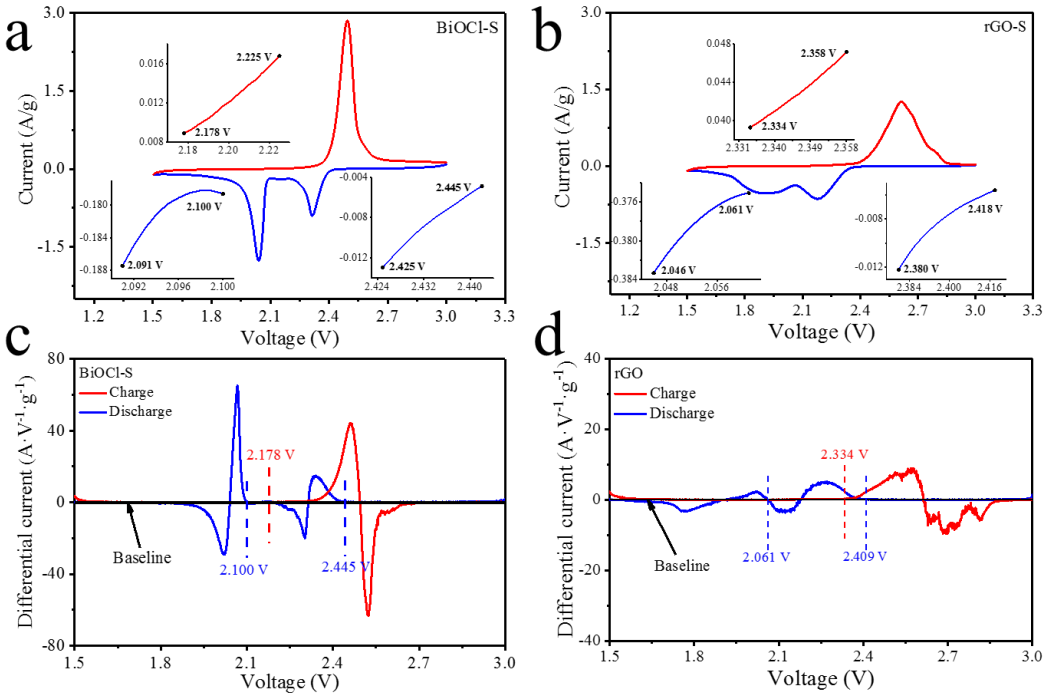

Figure S9. CV curves and onset potentials of redox peaks of (a) BiOCl/G-S and (b) rGO-S cathodes, and corresponding differential CV curves of (c) BiOCl/G-S and (d) rGO-S

cathodes.

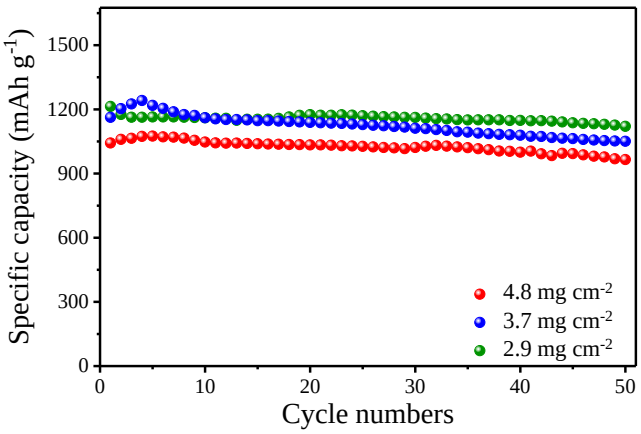

Figure S10. Cycle performance with different sulfur loading cathodes at 0.2 C.

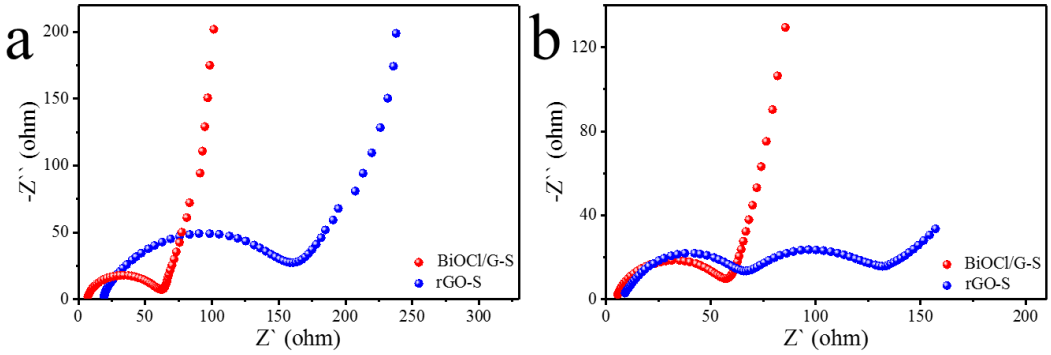

Figure S11. Nyquist plot of BiOCl/G-S and rGO-S cathodes (a) before and (b) after cycles.

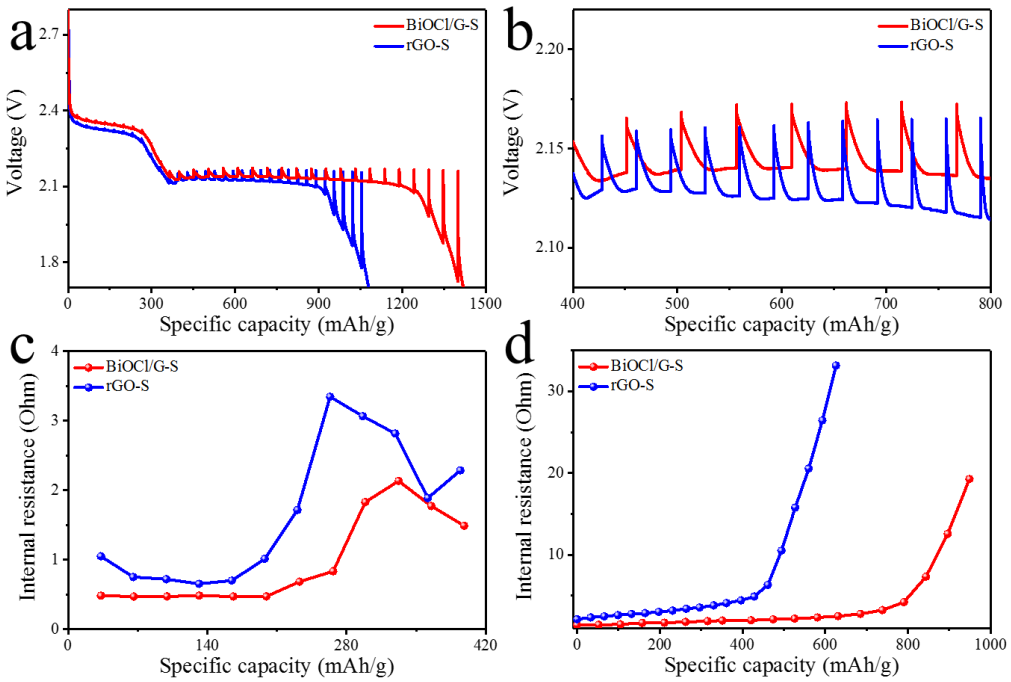

Figure S12. (a) GITT curves of BiOCl/G-S and rGO-S cathodes, and corresponding (b) magnified curves. (c, d) Internal resistance of different discharge plateaus with BiOCl/G-S

and rGO-S cathodes.

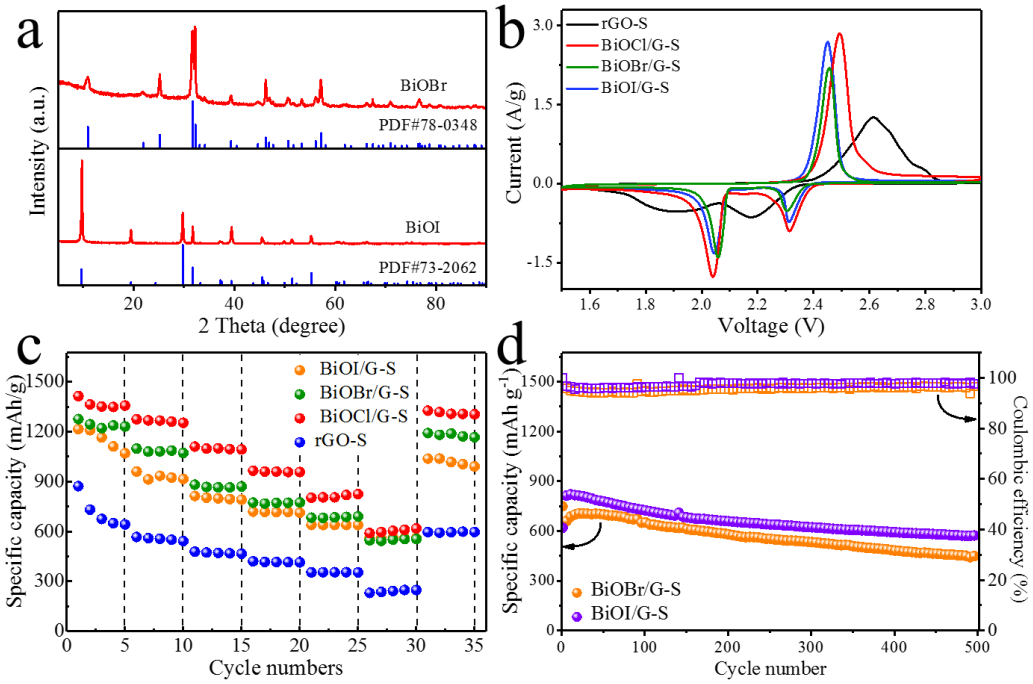

Figure S13. (a) XRD patterns of BiOBr and BIOI. (b) CV curves of rGO-S, BiOCl/G-S, BiOBr/G-S, and BiOI/G-S. (c) Rate performance of rGO-S, BiOCl/G-S, BiOBr/G-S, and BiOI/G-S. (d) Cycle stability test of BiOBr/G-S and BiOI/G-S at current density of 2 C.

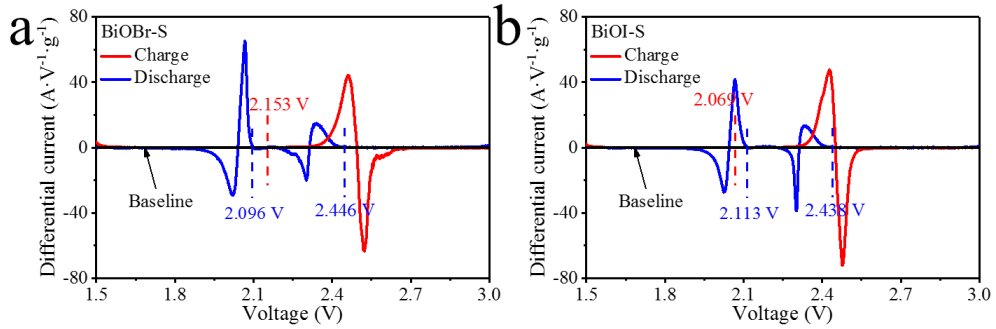

Figure S14. Differential CV curves of (a) BiOBr/G-S and (b) BiOI/G-S cathodes.

Table S1. Specific area and pore volume of BiOCl/G and rGO.

	BiOCl/G	rGO	BiOCl/G-S
Specific area (m^2/g)	117.0	81.7	1.1
Pore volume (cm^3/g)	0.105	0.073	0.016

Table S2. Electrochemical performances of BiOCl/G-S cathode compared with other representative sulfur cathodes.

Sulfur host	Sulfur content (wt.%)	Current rate (C)	Cycle number	Capacity (mAh/g)	Capacity decay rate (per cycle)	Ref.
MnO_2@H	67.9	~1.8	200	503	0.401%	1

CB						
PPy-MnO_2	70	1	500	850	0.07%	2
G-V_2O_3	62.6	2	1000	848	0.046%	3
ACNF/Co_3S_4	53	1	450	953	0.079%	4
NiS@C-HS	72	0.5	300	723	0.013%	5
MXene	70	0.5	650	1090	0.05%	6
CP-TiC	61	0.2	100	1032	0.351%	7
TiN	58.8	0.5	500	988	0.13%	8
Ni_2P-YS	65.1	1	500	1022	0.145%	9
BiOCl/G	69	0.2 1	100 2000	1217 1034	0.104% 0.007%	This work

Table S3. Onset potentials of redox peaks for different cathodes.

	Peak Ⅰ	Peak Ⅱ	Peak Ⅲ
rGO-S	2.061 V	2.409 V	2.334 V
BiOCl/G-S	2.100 V	2.445 V	2.178 V
BiOBr/G-S	2.096 V	2.444 V	2.153 V
BiOI/G-S	2.113 V	2.438 V	2.069 V

REFERENCE

1. Rehman, S.; Tang, T.; Ali, Z.; Huang, X.; Hou, Y. Integrated Design of MnO_2 @Carbon Hollow Nanoboxes to Synergistically Encapsulate Polysulfides for Empowering Lithium Sulfur Batteries. *Small* **2017**, 13, 1700087.

2. Zhang, J.; Shi, Y.; Ding, Y.; Zhang, W.; Yu, G. *In Situ* Reactive Synthesis of Polypyrrole-MnO_2 Coaxial Nanotubes as Sulfur Hosts for High-Performance Lithium-Sulfur Battery. *Nano Lett*. **2016**, 16, 7276-7281.

3. Song, Y.; Zhao, W.; Wei, N.; Zhang, L.; Ding, F.; Liu, Z.; Sun, J. *In-Situ* PECVD-Enabled Graphene-V_2O_3 Hybrid Host for Lithium-Sulfur Batteries. *Nano Energy* **2018**, 53, 432-439.

4. Xu, H.; Manthiram, A. Hollow Cobalt Sulfide Polyhedra-Enabled Long-Life, High

Areal-Capacity Lithium-Sulfur Batteries. *Nano Energy* **2017**, 33, 124-129.

5. Ye, C.; Zhang, L.; Guo, C.; Li, D.; Vasileff, A.; Wang, H.; Qiao, S.-Z. A 3D Hybrid of Chemically Coupled Nickel Sulfide and Hollow Carbon Spheres for High Performance Lithium-Sulfur Batteries. *Adv. Funct. Mater.* **2017**, 27, 1702524.

6. Liang, X.; Garsuch, A.; Nazar, L. F. Sulfur Cathodes Based on Conductive MXene Nanosheets for High-Performance Lithium-Sulfur Batteries. *Angew. Chem. In. Ed.* **2015**, 54, 3907-3911.

7. Peng, H. J.; Zhang, G.; Chen, X.; Zhang, Z. W.; Xu, W. T.; Huang, J. Q.; Zhang, Q. Enhanced Electrochemical Kinetics on Conductive Polar Mediators for Lithium-Sulfur Batteries. *Angew. Chem. In. Ed.* **2016**, 55, 1-6.

8. Cui, Z.; Zu, C.; Zhou, W.; Manthiram, A.; Goodenough, J. B. Mesoporous Titanium Nitride-Enabled Highly Stable Lithium-Sulfur Batteries. *Adv. Mater.* **2016**, 28, 6926-6931.

9. Cheng, J.; Zhao, D.; Fan, L.; Wu, X.; Wang, M.; Zhang, N.; Sun, K. Ultra-High Rate Li-S Batteries Based on a Novel Conductive Ni_2P Yolk–Shell Material as the Host for the S Cathode. *J. Mater. Chem. A* **2017**, 5, 14519-14524.